



Tuneable Resolution As a Systems Biology Approach for Multi-Scale, Multi-Compartment Computational Models

Denise E. Kirschner, Department of Microbiology and Immunology, Univ. of Michigan Medical School, Ann Arbor, MI

C. Anthony Hunt, Department of Bioengineering and Therapeutic Sciences, University of California, San Francisco, CA

Simeone Marino, Department of Microbiology and Immunology, Univ. of Michigan Medical School, Ann Arbor, MI

Mohammad Fallahi-Sichani, Department of Systems Biology, Harvard Medical School, Boston, MA

Jennifer J. Linderman, Department of Chemical Engineering, Univ. of Michigan, Ann Arbor, MI

Keywords: sensitivity analysis, agent-based model, virtual experiments, model linking, modularity, tuberculosis

Correspondence: kirschne@umich.edu; a.hunt@ucsf.edu; linderma@umich.edu

Abstract

The use of multi-scale mathematical and computational models to study complex biological processes is becoming increasingly productive. Multi-scale models span a range of spatial and/or temporal scales and can encompass multi-compartment (e.g. multi-organ) models. Modeling advances are enabling virtual experiments to explore and answer questions that are problematic to address in the wet-lab. Wet-lab experimental technologies now allow scientists to observe, measure, record, and analyze experiments focusing on different system aspects at a variety of biological scales. We need the technical ability to mirror that same flexibility in virtual experiments using multi-scale models. Here we present a new approach, tuneable resolution, which can begin providing that flexibility. Tuneable resolution involves fine- or coarse-graining existing multi-scale models at the user's discretion, allowing adjustment of the level of resolution specific to a question, an experiment, or a scale of interest. Tuneable resolution expands options for revising and validating mechanistic multi-scale models, can extend the longevity of multi-scale models, and may increase computational efficiency. The tuneable resolution approach can be applied to many model types, including differential equation, agent-based, and hybrid models. We demonstrate our tuneable resolution ideas with examples relevant to infectious disease modeling, illustrating key principles at work.

Introduction

Continued advances in biomedical science will require more explanatory mathematical and computational models (1-9). Increasingly these models are multi-scale, encompassing processes operating at a range of temporal and spatial scales and perhaps also between multiple compartments (e.g. organs). The key goal of multi-scale modeling in medically-focused systems biology is the generation of models that can be used to better understand hypothesized mechanisms, make predictions, interpret data, suggest new approaches for therapy, and offer new explanations for observed phenomena.

Advances in multi-scale modeling are enabling virtual experiments to answer questions that can be problematic to address in a wet-lab (10-15). In wet-lab experiments, advances in technology now allow scientists the flexibility to observe, measure, record, and analyze experiments at a variety of scales. We need the same capability in our virtual experiments (Figure 1). While virtual experiments cannot replace experimentation on living systems, they can be used to create new knowledge and improve explanatory insight. To do so, we develop, explore, and challenge alternative, plausible mechanistic scenarios, including hypotheses within and across scales. As progress is made, we can increase the synergy between virtual and wet-lab experiments. Such synergy is expected to be most productive as our multi-scale models become increasingly analogous to their animal model and human counterparts at multiple scales, under an expanding variety of intervention scenarios.

One strategy to achieving such flexibility and increasing the useability of multi-scale models is an approach we term *tunable resolution*. Tunable resolution proposes that multi-scale models should be built with multiple levels of resolution, so that a fine-grained or coarse-grained version can be employed with user discretion, allowing adjustment of the level(s) of resolution specific to a question, an experiment, a particular use, or a change in perspective or scale of interest. In addition to providing this flexibility of level of resolution, we argue that a tunable resolution approach expands options for revising and validating models and increases model usability and portability.

We describe our tunable resolution approach starting with arguments for, and evolving principles guiding, its use. We then demonstrate resolution tuning in models of the immune response to infection with *Mycobacterium tuberculosis*, the pathogen that causes tuberculosis (TB) (Examples 1 to 3). Despite many different and insightful experimental approaches taken over the years, fundamental questions remain about TB. In the TB context, virtual experiments provide means and strategies for generating and testing hypotheses about the disease, its mechanisms, and potential treatments (16).

The Argument for tuneable resolution

Tuneable resolution provides flexibility required to span varying aspects and scales of interest. Experiments on living systems often focus on a single aspect (or feature) and a single scale. Multiple types of experiments allow access to information at different scales. For example, images of diseased lungs provide information about the spread of TB, whereas immune responses developing in draining lymph nodes determine how well infection can be controlled. We need the flexibility and technical ability to change an aspect of a multi-scale model on which a new virtual experiment focuses and, when needed, the observation interval and frequency (Figure 2). We also need to retain essential knowledge when the aspect of interest changes, e.g., from signalling networks within an immune cell to immune cells interacting with each other. Models built with tuneable resolution can achieve this.

Tuneable resolution enables more comprehensive model validation. We can improve both explanatory and predictive usefulness by improving phenotypic overlap between phenomena generated by multi-scale models and their real world counterparts. To do so we must increase the variety of ways that results from virtual experiments can either be validated against corresponding wet-lab experiments or be objectively compared to available knowledge. We improve the scientific usefulness of multi-scale models by building trust into simulated mechanisms using a tuneable resolution approach and multiple validation targets. Trust increases in two ways: improving *in silico*-to-wet-lab similarities and identifying when, why, and where dissimilarities occur. We provide examples supporting our case that both activities require a tuneable resolution approach.

Fine-graining may present strategies for re-engineering to obtain an improved coarse-grained model. There are many computational and mathematical considerations that emphasize caution when adding fine-grain information to multi-scale models. A tuneable resolution approach argues not only for gradually and systematically building in additional detail into a model (as warranted by available data and questions being asked) but also for informing the formulation of a more biologically accurate coarse-grained version by using information from the fine-grained model. For example, an original coarse-grained model is developed and, because of further biological questions or additional validation targets, a finer-grained version is created (Figure 2, A1 → A2a → A3; Figure 2, B1 → B3). Once those questions are answered, the user wishes to return to a simpler representation but that preserves the biological integrity of the system (although not necessarily the mathematical integrity): a tuneable resolution approach provides a coarse-grained model that has been improved by insights gained during virtual experiments on the fine-grained model. This process helps one discover what mechanisms must appear in the model, and at what level of detail, to explain corresponding biological data (Figure 2, A3 → A2b). Put another way, the re-engineered coarse-grained model can be thought of as a “model of a model”, i.e. a version that retains some, but not all, finer-grained model behaviours.

Tuneable resolution can help identify model flaws. Models are perpetual works in progress. New insights, either from virtual or wet-lab experiments, can falsify one or more mechanistic model features, requiring model revision. The multiple perspectives offered by models capable of tuneable resolution may reduce bias and enable identifying the location of a model flaw, and thus can reduce reengineering required to produce and validate resulting revised and improved models.

Tuneable resolution may help identify the scale location of a “tipping point”. An overarching goal for biomedical research is discovery of new intervention strategies that improve health outcomes. For TB, diabetes, cardiovascular diseases and others that are still shrouded in considerable uncertainty, the scale location of the tipping point for a therapeutic intervention under study can be unknown and may even vary between individuals. For example, should a therapy target a specific receptor/ligand interaction in a specific biological organ, the expansion of a class of T cells, or are both required but following a coordinated strategy? We envision that virtual experiments using tuneable resolution provide new options for expediting and narrowing the search. This would arise, for example, when creating a new coarse grained sub-model to replace a fine-grained sub-model (Figure 2). Key model mechanisms that are required to preserve the behaviour obtained with the fine-grained are likely tipping points for the combined multi-scale model behaviour. In a nonlinear ordinary differential equation (ODE) system, for example, those necessary preserved behaviours may identify bifurcation parameters that are targets for therapeutic interventions.

Tuneable resolution approaches can increase computational speed, model usefulness and portability. Most multi-scale models grow in complexity and scope as researchers add mechanisms and detail to improve agreement and usefulness in interpreting experimental data. Consequently, the model can become increasingly difficult to work with – more difficult to debug, to port to other platforms and other users – and the results of virtual experiments may become more difficult to interpret. Simulations may require significantly longer runtimes. Indeed, some models essentially “die” under their own weight, becoming too complex to be passed on to the next user. Tuneable resolution approaches, particularly those emphasizing modularity, model linking and re-engineering of coarse-grained model versions, can assist in avoiding or reducing these problems.

Evolving principles for building tuneable resolution models

Resolution tuning requires coupled use of coarse- and fine-graining methods. Our model development typically proceeds by first including well-studied and characterized processes known to have major or first-order effects on system behaviour. Given specific questions to be addressed in virtual experiments, some biological processes may not require great detail in their description, and so can be represented in a coarse-grained fashion, e.g. using a parameter or a simple phenomenological expression. New biological questions or data might later require

virtual experiments that have a new focus and new multi-scale model uses, and that, in turn, may require increased model resolution, or fine-graining, e.g. replacing the parameter or simple phenomenological expression with a sub-model that simulates relevant biological processes in greater detail. Adding information from multiple length and time scales, while important for simulating phenomena, significantly increases the complexity of analyses and execution time. Thus it is important to be able to selectively (and possibly automatically) coarse-grain model components and/or features when needed. Coarse-graining can be achieved by replacing a sub-model consisting of several biologically based equations or rules with wisely-chosen phenomenological expressions (e.g. a parameter, a function, or a simplified model). These choices may be guided by temporal considerations (e.g., pseudo steady state assumption), by validation targets, and/or by information obtained during building and execution of the fine-grained model. Note that there is no single method for coarse- or fine-graining, and strategies vary by field. Various model structures will require different methods and a review of these methods is beyond the scope of this review.

Tuneable resolution can be used with different multi-scale model constructs. Multi-scale models with similar uses can have different constructs, including ODE, partial differential equation (PDE), stochastic, object- and agent-based, and hybrid (i.e. models combining different constructs) (e.g. (17-26)). Consequently there is no single strategy for achieving tuneable resolution. Regardless of construct type, it is important to have the ability to shift the aspect and/or scale of focus at will. In Examples 1 and 2, we demonstrate tuneable resolution using hybrid models that combine non-linear systems of ODEs as sub-models that fine-grain mechanisms of an agent-based model (ABM). In addition, organ compartments of interest can be represented using either coarse- or fine-grained versions as appropriate for the particular virtual experiment (Example 3).

Model linking is central to tuneable resolution. Resolution tuning and established multi-resolution modeling methods face several similar technical, implementation, computational, and mathematical issues. Interfacing or linking independent model components that operate at different temporal or spatial granularities is a prominent example (27-29). Interfacing or linking independent model components that use different modes of computation (e.g., agent-based and continuous mathematics) is another. Adjusting the resolution in a model requires explicit consideration of model linking issues. There are no standard linking methods. Although details are beyond the scope of this communication, we note that several groups are developing frameworks to modularize models to improve model linking with an eye toward efficient model (7-9, 30-38). For example, the multi-scale modelling platforms CompuCell 3D (www.compcell3d.org), Simmune, and Virtual Cell (<http://www.ibiblio.org/virtualcell/>) all provide approaches for model linking (39-41).

Modularity becomes necessary, even essential. Another impediment in the quest for improved multi-scale models is that they can become so complicated that scientific

utility is jeopardized. The cost to copy, verify, and maintain their operation can be prohibitive. In addition, considerable specialized expertise and training is needed to conduct virtual experiments using current multi-scale models. Finally, the barrier to independent virtual experiment replication (as distinct from repetition) becomes too great (42-47). Our experience is that because model variants identified during virtual experiments employing tuneable resolution are somewhat specialized, they can be easier to share and have shorter learning curves. There is value to moving in the direction of multi-scale models designed intentionally to be modular at all scales, where module variants having the same biological counterpart but different mechanistic granularities can be exchanged with biomimetic fidelity and confidence both within and between experiments. As these modules become more long-lived, our expectation is that it will become increasingly easy to replicate virtual experiments (a standard in science), and that barriers to more widespread use of virtual experiments will be lowered. Research to improve model modularity is an actively expanding activity

(http://www.imagwiki.nibib.nih.gov/mediawiki/index.php?title=Main_Page).

Uncertainty and sensitivity analyses play important, and multiple, roles in tuneable resolution. When data are not available to determine some model parameter values, uncertainty and sensitivity analyses can be used to investigate, narrow and define parameter spaces. Key, generalized features of the process are illustrated in Figure 3. The first role for uncertainty analysis is to assess the uncertainty in model output that results from uncertainty in parameter values. Common techniques include generalized Monte Carlo methods (e.g., simple random sampling, Latin hypercube sampling) (48). Sensitivity analysis is then used to quantify how parameter uncertainty impacts model outcomes and to identify critical model parameters. Common techniques include generalized correlation (e.g., partial rank correlation coefficients) and variance decomposition methods (e.g., ANOVA, fast Fourier transform) (48). The second role for uncertainty and sensitivity analyses in tuneable resolution is to identify key mechanism features to guide fine-graining and sub-model development. For example, we can fine-grain a model by adding detail to processes suggested by sensitivity analysis as significant or we can coarse-grain by conflating sets of parameters that do not have a large impact on model outcome. Most sensitivity analysis techniques supply indices that are time-dependent; key regulatory mechanisms can be important only during certain—sometimes narrow—time intervals. Such time-dependency can also be exploited to guide when to change resolution in an automated fashion. For example, if sensitivity analysis suggests that a certain mechanism is only important early, then we can use the fine-grain model version early during the virtual experiment and, based on set criteria, switch to a coarse-grain version thereafter (49). That illustration highlights that tuneable resolution can be applied temporally as well as spatially. Finally, we use uncertainty and sensitivity analyses for estimating new parameter values when toggling between coarse- and fine-grained model versions (i.e. tuneable resolution)

to maintain biological fidelity and model congruency with regard to key biological features (Figure 3).

Tuneable resolution is distinguishable from multi-resolution modeling. Multi-resolution modeling refers to building a single model, a family of models, or both to describe the same phenomena at different levels of resolution, across multiple scales. Multi-resolution modeling has a rich history in other domains, most notably conflict and combat modeling (50-54) and ecology (55-58). However, two important characteristics distinguish many of those models from the tuneable resolution approach described here. First, multi-resolution modeling efforts typically adopt a reductionist, bottom-up approach, assuming that knowledge, measurements, and data are available to achieve an acceptable degree of biological validation at the finest grain (Figure 4, right side) (59, 60); modelling typically begins with mathematical descriptions of multi-level mechanisms that are physics-based. Yet, for TB and many other medical fields, the fine grain, explanatory, mechanistic knowledge needed to build a classical multi-resolution model is still not available, placing us toward the green area of Figure 4. In fact, a primary goal in our research has been to use virtual experiments to facilitate acquiring this knowledge. We have begun with rather coarse-grained models, refining them to generate biomimetic phenomena, and then focused “downward” to discover plausible, finer-grained mechanistic generators to improve insight into the mechanisms operating at the level above. This process is what Brenner and Noble describe as the “middle out” approach (61).

Second, a key use for multi-resolution modelling is generating fast and accurate predictions, and the focus is on inductive and deductive reasoning. Our interest is different: models and methods were needed to enable mechanistic exploration and subsequent development of improved explanations of phenomena (7, 62-64) including improved phenotype overlap (Fig. 3). Improving insight requires shifting the aspect of focus of new virtual experiments, i.e. resolution tuning, in ways not easily anticipated. Those activities require expanding the range of reasoning methods used to include analogical (65) and abductive reasoning (7, 63, 64). (Figure 4).

Model reduction is distinguishable from tuneable resolution. Model reduction is an approach that has been used for coarse-graining models. Although some theoretical and ad-hoc methods have been used to reduce differential equation models, e.g. (66-68), there is no standard method yet available, particularly when dealing with multi-scale or multiple linked models of different types (e.g. hybrid models). Model reduction is guided primarily by mathematical considerations (e.g. singular perturbation analysis, non-dimensionalization), while resolution tuning is guided primarily by biological considerations and questions (e.g. a need to consider as yet unexplored molecular events, or an interest in focusing on another aspect of the system). That said, model reduction and a tuneable resolution approach may in some cases lead to a similar outcome, even if motivated by very different objectives.

Example 1: Tuneable resolution implemented for a key cytokine in a model of a lung granuloma in tuberculosis

The key pathologic feature of TB is the formation of granulomas, self-organizing aggregates of immune cells and *M. tuberculosis* within lungs (Figure 5A). Most granulomas are capable of containing bacterial infection, leading to (in humans) a clinically latent infection that may last for years. If, however, granulomas are impaired in function, infection can progress, granulomas enlarge, and bacteria seed new granulomas; this sequence causes progressive pathology, i.e. active TB disease. How the interplay between various biological processes results in different infection outcomes is not known, but it is clear that granulomas play a central role. Myriad host factors operating within and across length and time scales influence granuloma formation and function and thus infection outcome. Improved understanding of mechanisms responsible for granuloma dynamics is expected to lead to new therapeutic strategies. Because multi-scale models can simultaneously incorporate host-pathogen interactions occurring over molecular, cellular and tissue scales, they are well-suited for exploration of the immune response to *M. tuberculosis* infection.

In this example, we demonstrate tuneable resolution by introducing a multi-scale model of granuloma formation and function, fine-graining that model to include molecular level detail, and then re-engineering the original model guided by insights “learned” from experiments using the fine-grained version.

GRANSIM is our agent-based model (ABM) describing granuloma formation and function in lungs during *M. tuberculosis* infection and focusing on cellular and tissue scale dynamics (69, 70) (Figures 5B and 6A). Immune cells (resting, infected, chronically infected, and activated macrophages; regulatory, cytotoxic, and interferon- γ (IFN- γ)-producing T cells) are represented as discrete agents. Effector molecules (such as IFN- γ) and bacteria (extracellular, intracellular, and non-replicating bacteria) are represented using continuous variables. Each simulation follows granuloma formation and function over several hundred days, building over time to track thousands of individual cells (agents). *GRANSIM* (and the related models described here) were developed and achieved degrees of validation utilizing extensive data from mice and primates. Simulated granuloma features map to the wide spectrum of those observed in primates, including bacterial containment, clearance (sometimes with extensive inflammation), and dissemination.

GRANSIM includes only minimal information regarding an important pro-inflammatory cytokine, tumor necrosis factor- α (TNF). TNF is produced by infected and activated macrophages as a membrane-bound precursor (mTNF) that can be cleaved and released as a soluble protein (sTNF) (71, 72). TNF binding to membrane receptors (TNFR1 and TNFR2) affects the immune response to bacteria

through several mechanisms, including activation of macrophages to more effectively kill bacteria, induction of chemokine and cytokine expression, and modulation of apoptosis (73-75). In humans and non-human primates, TNF neutralization leads to reactivation TB, i.e. the appearance of active disease where it was once latent, due to a failure of granulomas to control bacterial replication (76-79). Therefore, TNF availability and activities within granulomas are essential for restricting bacterial growth (80) and maintaining a latent infection.

Availability of TNF within granulomas is controlled not only by the rate of TNF secretion from macrophages and TNF degradation in tissue, but also by receptor binding and trafficking (i.e. receptor internalization, degradation, recycling, and shedding) processes. Results of uncertainty and sensitivity analyses demonstrated the significance of changes in TNF availability in granuloma function during *GRANSIM* simulations, highlighting the likely key role of TNF-related processes in controlling actual infections. *GRANSIM*, however, does not include a representation of the receptor-level processes believed to control cellular responses and TNF availability. To improve insight into current theories of TNF-related mechanisms and discover new options for targeting granulomas therapeutically, we incorporated TNF-related molecular-scale details and mechanisms within *GRANSIM*, terming the resulting fine-grained version *GRANSIM_{TNF}*. (Figure 6B, C) (11, 81). Molecular scale dynamics of TNF/receptor binding and trafficking processes were represented as a sub-model with a nine non-linear ODE system solved individually for each cell agent (i.e. macrophage or T cell – equating to several thousand agents per simulation). Simultaneously, the solution to the PDE describing TNF diffusion at the cellular scale on the grid is computed, thus linking soluble TNF concentrations at the cellular/tissue scales to TNF binding and trafficking events within individual cells.

TNF activates two major signaling pathways, the caspase-mediated apoptotic and the NF-κB pathways. In *GRANSIM_{TNF}* we coarse-grain both these pathways, linking the outputs solely to bound TNF receptors (see Example 2 for an option that includes detail in one of the pathways) (11). TNF-induced NF-κB activation for each individual macrophage is described as a Poisson process with a probability that is a function of the NF-κB activation rate constant ($k_{NF-\kappa B}$), the concentration of TNF-bound cell surface TNFR1 complexes [C], and a threshold for those complexes ($\tau_{NF-\kappa B}$):

$$P_{NF-\kappa B} = \begin{cases} 0 & ; [C] < \tau_{NF-\kappa B} \\ 1 - e^{-k_{NF-\kappa B}([C] - \tau_{NF-\kappa B})\Delta t} & ; [C] \geq \tau_{NF-\kappa B} \end{cases} \quad (1)$$

An NF-κB-activated macrophage secretes chemokines and TNF, and can be activated to kill bacteria. The probability of TNF-induced apoptosis for each individual cell is specified by:

$$P_{apopt} = \begin{cases} 0 & ; [C_i] < \tau_{apopt} \\ 1 - e^{-k_{apopt}([C_i] - \tau_{apopt})\Delta t} & ; [C_i] \geq \tau_{apopt} \end{cases} \quad (2)$$

P_{apopt} is a function of the apoptosis rate constant (k_{apopt}), internalized TNF-bound TNFR1 complexes [C_i], and a threshold for those complexes (τ_{apopt}). Equations 1 and 2 link TNF/receptor binding and interactions to cellular scale processes.

A key $GRANSIM_{TNF}$ prediction is that soluble TNF gradients form within granulomas. High concentrations of soluble TNF near the center of the granuloma give way to lower peripheral concentrations. Although the prediction cannot yet be validated against wet-lab data, the consequences are provocative. High central levels of TNF should trigger apoptosis of infected macrophages, whereas lower levels at the periphery should trigger survival pathways for T cells, which are needed to fight infection (81). Uncertainty and sensitivity analyses allowed us to identify how TNF/TNFR binding and trafficking dynamics may control the soluble TNF gradient (11). $GRANSIM_{TNF}$ can also be used to explore effects of potential pharmacological manipulation of TNF receptor binding and trafficking (82). For example, the TNFR1 internalization rate constant controls the spatial range of TNF action in a simulated granuloma (11); TNFR1 internalization kinetics represent a “tipping point” identified by varying model resolution. Small internalization rates lead to a greater chance of clearance of the infection, but at the expense of excessive inflammation due to high TNF concentrations (Figure 7). Virtual experiments suggest that latent TB represents a physiological compromise that avoids more destructive outcomes (83).

The fine-graining of our base model to include TNF/TNF receptor binding and trafficking and TNF-driven cell behavior was well-motivated by a desire to understand the important roles that TNF plays in granuloma formation and function. However, when the focus of our virtual experiments shifts to a new system aspect, for example the role of a different cytokine or cell type, or the effect of a TNF knockout, the model may not need extensive detail regarding TNF. Yet we would like to retain what we learned during the fine-graining to create $GRANSIM_{TNF}$. Thus we used a tuneable resolution approach, learning from $GRANSIM_{TNF}$ to re-engineer $GRANSIM$ (Figure 6B), at least with respect to TNF. Because our analyses demonstrated the importance of the TNFR1 internalization to the fine-grained model outcomes, we replaced the nine ODEs describing TNF receptor binding and trafficking (11) with this single ODE:

$$\frac{d[sTNF]}{dt} = k'_{synth} - \left(\frac{[sTNF]}{[sTNF] + K_{d1}} \right) k_{consumption} \quad (3)$$

Equation 3 describes the change of soluble TNF concentration within an ABM compartment that contains a macrophage or T cell; k'_{synth} is the rate of sTNF secretion by the immune cell, and $k_{consumption}$ is the apparent rate constant for sTNF

consumption (i.e. by internalization). The factor $\frac{[sTNF]}{[sTNF] + K_{d1}}$ represents the sTNF-bound fraction of TNFR1s on membranes of immune cells (assuming a pseudo steady-state). K_{d1} is TNFR1 affinity for sTNF. Because the ODEs are being solved for each of the thousands of agents (cells) during simulation, replacing nine ODEs with a single ODE yields significant computational savings (simulation times, on the order of tens of minutes, are cut roughly in half). Note that because these are stochastic simulations, and because it is also necessary to run uncertainty and sensitivity analyses, thousands of simulations are required for full analysis of the model.

In addition, Eqns. 1 and 2 are replaced with equations that rely on the extracellular sTNF concentration rather than bound TNFR1 receptors for probability computations:

$$P_{NF-\kappa B} = \begin{cases} 0 & ; \frac{[sTNF]}{[sTNF] + K_{d1}} < \tau'_{NF-\kappa B} \\ 1 - e^{-k'_{NF-\kappa B}(\frac{[sTNF]}{[sTNF] + K_{d1}} - \tau'_{NF-\kappa B})\Delta t} & ; \frac{[sTNF]}{[sTNF] + K_{d1}} \geq \tau'_{NF-\kappa B} \end{cases} \quad (4)$$

$$P_{apopt} = \begin{cases} 0 & ; \frac{[sTNF]}{[sTNF] + K_{d1}} < \tau'_{apopt} \\ 1 - e^{-k'_{apopt}(\frac{[sTNF]}{[sTNF] + K_{d1}} - \tau'_{apopt})\Delta t} & ; \frac{[sTNF]}{[sTNF] + K_{d1}} \geq \tau'_{apopt} \end{cases} \quad (5)$$

where $k'_{NF-\kappa B}$, k'_{apopt} , $\tau'_{NF-\kappa B}$ and τ'_{apopt} are modified rate constants and thresholds for TNF-induced NF-κB activation and apoptosis, respectively. Because TNF-induced responses (NF-κB activation and apoptosis) in immune cells actually result from sTNF binding to TNFRs on the cell membrane, TNF concentration thresholds $\tau'_{NF-\kappa B}$ and τ'_{apopt} in Eqns. 4 and 5 are defined based on $\frac{[sTNF]}{[sTNF] + K_{d1}}$. Initial estimates of

the values of the new model parameters (k'_{synth} , $k_{consumption}$, $k'_{NF-\kappa B}$, k'_{apopt} , $\tau'_{NF-\kappa B}$ and τ'_{apopt}) are based on related parameters from GRANSIM_{TNF}. For example, knowing the rate constant for TNFR internalization and the average number of cell surface TNFRs, we estimated a suitable range of values for $k_{consumption}$ to be on the order of $k_{int1}[TNFR1]$, where k_{int1} is the TNFR1 internalization rate constant.

The resulting re-engineered GRANSIM now also predicts TNF concentration gradients are present within a granuloma and thus lower levels of macrophage activation and inflammation occur at the periphery of granuloma, improving similarities with experimental data. Depending on the focus of a virtual experiment,

we can now toggle between $GRANSIM_{TNF}$ and the re-engineered $GRANSIM$ (BOX), exercising resolution tuning and, in the case of $GRANSIM$, incorporating information regarding molecular-level TNF without the computational expense and complexity of the full model.

Example 2: Tuneable resolution implemented for NF- κ B signaling in a model of a lung granuloma in tuberculosis

In Example 1, we introduced $GRANSIM_{TNF}$, a hybrid multi-scale model (consisting of agent-based, ODE, and PDE models) that simulates the immune responses – specifically, granuloma formation and function – during infection with *M. tuberculosis* (Figure 6A,C). Although this model captures receptor binding and trafficking processes that in part control TNF availability, it contains limited detail regarding the biological mechanisms that determine the relationship between TNF-bound receptors and cellular responses (Eqn. 1). In this example, we demonstrate tuneable resolution, fine-graining $GRANSIM_{TNF}$ by incorporating additional molecular detail describing one of the intracellular signalling pathways elicited by TNF binding and then re-engineering $GRANSIM_{TNF}$ to increase biomimetic fidelity.

TNF binding initiates a signaling pathway leading to translocation of NF- κ B into the nucleus and ultimately transcription of target inflammatory genes. Activation of the NF- κ B pathway affects the immune response to *M. tuberculosis* through (at least) four mechanisms in macrophages: activation to efficiently kill bacteria, induction of chemokine secretion, induction of cytokine (TNF) expression, and inhibition of apoptosis (73-75, 84-87). We wanted to use virtual experiments to explore answers to questions that would require TNF signaling granularity greater than that in $GRANSIM_{TNF}$. For example, how do the dynamics of the TNF-induced NF- κ B pathway influence the long-term immune response to bacteria? Could targeting the TNF-induced NF- κ B pathway affect granuloma formation and function? To undertake those virtual experiments we developed a new (and finer-grained) version of $GRANSIM_{TNF}$, termed $GRANSIM_{TNF-NFKB}$, containing the enhanced intracellular component details illustrated in Figure 6D (82).

Recent cell culture experiments, including those in (88), have identified important molecular mechanisms controlling the dynamics of NF- κ B signaling at the single-cell level. To explore possible influences of this pathway in the context of host infection, we incorporated a representation of these dynamics into our model. Equation 1 was replaced by a set of 50 nonlinear ODEs that determine NF- κ B signaling dynamics following TNF binding to cell surface TNF receptors (82, 88). Those NF- κ B dynamics were then linked to the four NF- κ B-mediated cell responses in macrophages listed above. NF- κ B-induced expression of genes corresponding to TNF, different chemokines, a generic inhibitor of apoptosis protein (IAP) (89), and a generic macrophage-activating molecule (ACT; representing, for example, proteins

involved in maturation of phago-lysosomes essential for killing bacteria (84)) as well as translation of their mRNA transcripts were represented using ODEs. For TNF and chemokines, ODEs also describe secretion to extracellular spaces. For macrophage activation and inhibition of apoptosis, because these processes are discrete at the single cell-level, cell behavior was described by a Poisson process with a probability determined within each time-step in part by the intracellular concentration of ACT and IAP, similar to Eqns. 1 and 2 (82). Fine-graining NF- κ B dynamics has two major effects on how TNF signaling is implemented. First, the higher resolution model (Figure 6A,D) is able to capture the dynamics of TNF-induced responses, for example, oscillatory expression of chemokines, as explored in (82). It also mathematically uncouples the four different NF- κ B mediated responses, which is appropriate as these processes are regulated by separate mechanisms (transcription and translation of distinct genes and mRNA transcripts). Virtual experiments using $GRANSIM_{TNF-NFKB}$ documented that the dynamics of TNF-induced NF- κ B-mediated responses are critical to controlling bacterial load, inflammation levels and granuloma size (82) (Figure 7).

The three model versions, $GRANSIM$, $GRANSIM_{TNF}$, and $GRANSIM_{TNF-NFKB}$, correspond to the coarse-, intermediate- and fine-grained multi-scale model versions shown schematically in Figure 2 (panels A1, A2a, and A3, respectively) and our tuneable resolution implementation is described in BOX. Model congruency between two of those versions in terms of key biological outcomes is shown schematically in Figure 7 and was obtained using uncertainty and sensitivity analysis (Figure 3). Although $GRANSIM_{TNF-NFKB}$ is the most detailed model, not all our questions regarding TB granuloma formation and function require this level of detail in the NF- κ B pathway. Thus, our next goal was to re-engineer and improve scientific usefulness of $GRANSIM_{TNF}$ by drawing on insights gained from $GRANSIM_{TNF-NFKB}$ (Figure 2, panel A2b).

Analysis of $GRANSIM_{TNF-NFKB}$ simulations showed that the timing of NF- κ B induced macrophage activation has a more significant effect on granuloma function than the timing of other responses, so we modified $GRANSIM_{TNF}$ to capture the timing effects for different NF- κ B mediated responses in a coarse-grained manner without solving for all reactions. The timing of all NF- κ B mediated responses in $GRANSIM_{TNF}$ is controlled by a single parameter $k_{NF-\kappa B}$, the NF- κ B activation rate constant, as described in Eqn. (1). We replaced this parameter with three independent parameters, $k_{activation}$, $k_{chemokine}$, and k_{TNF} , controlling the timing of each individual NF- κ B mediated response separately (k_{apopt} , controlling the rate of apoptosis, already exists in $GRANSIM_{TNF}$). These parameters control the probability of each NF- κ B associated response within a simulation time-step. For example, Eqn. (1) is modified to describe the probability at which a macrophage becomes capable of secreting chemokines following NF- κ B activation:

$$P_{chemokine} = \begin{cases} 0 & ; [C] < \tau_{NF-\kappa B} \\ 1 - e^{-k_{chemokine}([C] - \tau_{NF-\kappa B})\Delta t} & ; [C] \geq \tau_{NF-\kappa B} \end{cases} \quad (6)$$

Similar to Example 1, because the ODEs are being solved for each of the thousands of agents (cells) in the simulation, replacing 50 ODEs determining NF- κ B signaling dynamics with three ODEs yields significant computational savings (simulation times, on the order of several hours, are cut to tens of minutes). Because these too are stochastic simulations, thousands of simulations are required for uncertainty and sensitivity analyses.

Simulation results from the re-engineered $GRANSIM_{TNF}$ (Figure 8) show the importance of $k_{activation}$ compared to less significant effects of $k_{chemokine}$ and k_{TNF} on controlling bacteria numbers and the level of inflammation in tissue. These results also show model congruency between $GRANSIM_{TNF}$ and $GRANSIM_{TNF-NFKB}$ regarding the importance of the timing of macrophage activation in control of granuloma formation and functioning. Depending on the focus of our virtual experiments regarding TNF and its influence on granuloma dynamics, we can now toggle between a re-engineered $GRANSIM_{TNF}$ and $GRANSIM_{TNF-NFKB}$ (BOX), exercising resolution tuning and, in the case of $GRANSIM_{TNF}$, incorporating information from molecular-level NF- κ B simulations without the computational expense and complexity of simulating the full model.

Example 3: Tuneable resolution implemented for a multi-organ model of lung granuloma formation and function in tuberculosis

In Examples 1 and 2, the multi-scale models created added molecular scale dynamics to a cellular/tissue scale model. In this example, we highlight a tuneable resolution approach when fine-graining at the same scale as the original model. Another way to describe this is that we add an additional compartment (organ) to the original model.

Recruitment of immune cells to the lung to participate in control of infection is a critical event in granuloma formation during infection with *M. tuberculosis*. Recruited cells include T cells, macrophages and dendritic cells. Effector immune cells such as CD4+ and CD8+ T cells are generated in lymph nodes (LN) and must travel to lungs. The process can take anywhere from a few days to weeks for persistent pathogens like *M. tuberculosis*. Some studies show that an effective protective response to *M. tuberculosis* can be impacted by this slow or delayed induction or function of effector cells (90). For example, host-bacteria interactions can result in a delayed cell migratory activity or reduced antigen-presenting cell function, at least in macrophages (91-93). In addition, timing of initiation of granuloma formation (which is dependent on the recruitment of these effector cells from LN) can affect capabilities of antigen-presenting cells (such as macrophages and dendritic cells) to

find bacteria and migrate to draining LNs in a timely manner. Effector T cells are generated, but in most cases it is too late to allow infection to be cleared. Instead, there is either a “stand-off” leading to latency or an active infection. Clearly, LN dynamics can have a huge impact on the immune response to *M. tuberculosis* infection, and that is the focus of Example 3.

GRANSIM is low-resolution with respect to LN mechanisms and processes (Figure 6A, E and Examples 1 and 2) (11, 69, 70, 83). It captures effector T cell recruitment into the lung in a simplified way: by specifying a forcing function with a parameter representing the time of arrival of those cells to the lung. Decisions to recruit cells and what T cell phenotypes to recruit are based on events unfolding during simulations. Effector T cell phenotypes are defined based on their immunological functions: interferon- γ (IFN- γ)-producing T cells ($T\gamma$), cytotoxic T cells (T_c) and regulatory T cells (T_{reg}). T cell recruitment from LN to lung is a stochastic event, and occurs at specific sites (vascular sources) on the grid. To mimic the biological delay in adaptive immunity development in LNs, effector T cell recruitment is enabled only after ~20 days post infection, which reflects the typical 2-4 week post-infection ‘delay’ in mounting adaptive immunity. Uncertainty and sensitivity analyses show that simulated granuloma formation is highly dependent on the value of this delay parameter (69, 70), motivating a more physiologically realistic treatment of immune cell recruitment to the lung.

To better represent mechanisms occurring within a LN during granuloma formation, we fine-grained recruitment of immune cells from the LN by replacing parameters with an entire physiological compartment representing a LN (94) (Figure 6F, and schematically shown in Figure 2 panels B1 to B2). So doing allowed us to address questions related to modulation and timing of T cell responses as a function of infection progression within the lung. We mapped a single virtual LN to a collection of several (~5) lung-draining LNs, the sites of generation of effector T cells. The resulting multi-organ model, *GRANSIM-LN*, is hybrid: an ABM for the lung compartment (Figure 6A) and a non-linear system of ODEs representing phenomena within the LN compartment (Figure 6F) (94). The LN model includes mechanisms that represent antigen presentation and T cell priming and differentiation and consists of 13 ODEs tracking APCs, naïve T cells, and precursor and effector CD4+ and CD8+ T cells. Effector T cells can leave the LN to migrate to lungs. This LN model was developed and calibrated using data from *M. tuberculosis*-infected mice (95).

Linking the LN and lung granuloma models to form *GRANSIM-LN* requires specifying how cells traffic between the compartments. To represent T cell recruitment that is based on the level of infection in the lung, we used the scaled sum of infected and chronically infected macrophage populations in the lung to represent the pool of antigen-presenting cells that have potential to migrate to draining LNs. The biological behaviour to which this maps captures bacteria in lung causing more antigen-presenting cells to ingest them and traffic to LNs. Mathematical scaling is necessary

because *GRANSIM* represents only a portion of the lung, and our LN model represents only a single draining LN. We also account for delays that an antigen-presenting cell can encounter during uptake, maturation and migration processes between physiological compartments. The scaled sum of all infected macrophages in the lung at each time step is used as the initial condition for the “mature dendritic cell” (the key antigen-presenting cell in our model) equation within the LN. After the dynamics simulate for that time step in the LN model, T cells generated return to the lung via blood to participate in the lung infection model (*GRANSIM*). T cell fluxes generated by the LN model are converted into integers and cells are placed on a queue to enter the lung when a source location becomes available. A T cell in the queue has a fixed lifespan. Its “age” is preserved when it enters the grid. The process is intended to mimic the effect of effector T cells circulating through the blood and waiting for signals to extravasate into the tissue (96). The only recruitment parameter shared between coarse- and fine-grained model versions, *GRANSIM* and *GRANSIM-LN*, respectively, is a fixed threshold for recruitment of T cells that is based on the concentration of cytokines and chemokines at the blood sources, where cells can enter.

Using our fine-grained model, *GRANSIM-LN*, we can explore possible changes in the efficiency and magnitude of T cell priming, differentiation and migration to the lung. We can also capture the contraction phase of effector T cell fluxes due to a reduction of antigen-presenting cells migrating to LNs.

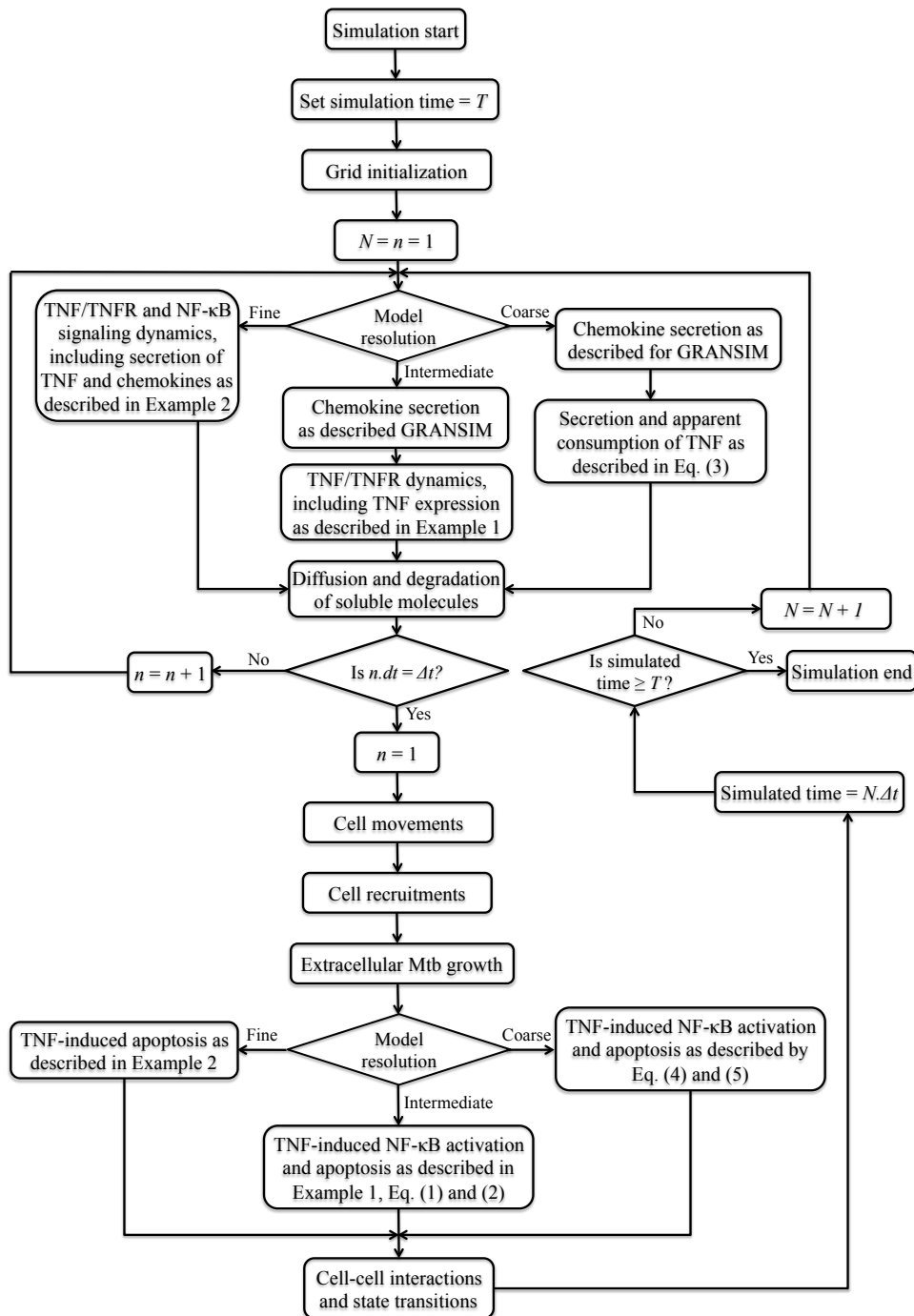
A key, virtual, *GRANSIM-LN* experiment demonstrated that detectable levels of effector T cells at the site of infection occur only above a threshold number of bacteria in the lung. Based on that observation, we re-engineered the original *GRANSIM* by introducing a new threshold parameter. When total bacteria counts in the lung ABM are greater than this threshold, T cell recruitment is enabled. To create this re-engineered *GRANSIM*, we focused on one of the most informative proxies for infection in the lung, the total bacteria count. We used measures from *GRANSIM-LN* to create a proxy function of total bacteria versus T cell fluxes from LN to lung. In order to simulate a large spectrum of granuloma outcomes ranging from clearance to dissemination, we varied 12 *GRANSIM* parameters (while fixing the LN model parameters) and generated 900 different temporal bacteria profiles. We plotted daily bacteria counts versus T cell flux (Figure 9; only T_γ fluxes are displayed). Figure 9A shows a clear separation of fluxes as infection progresses. We then fit time-adjusted functions to the data (Figure 9B) and generated an improved *GRANSIM* (Figure 9C).

Thus we have two model versions, in terms of incorporation of LN dynamics, the re-engineered *GRANSIM* and the fine-grained *GRANSIM-LN*; we can choose the appropriate version for the biological aspect of interest. (When needed, we also have a LN ABM that tracks individual cell movements and generation of effector T cells within a LN, but its details are beyond the scope of this example (49, 97-99)).

Our tuneable resolution approach gives us the ability to toggle easily between different model versions to continually improve explanatory mechanistic insights and expand the scope of those insights. That process is illustrated by the data in Figure 10. Results from the re-engineered *GRANSIM* differ from the other resolutions: using the same set of parameter values shared across versions, it returns more total bacteria in the range of 0-1000 (Figure 10A). This demonstrates that the original *GRANSIM* formulation of T cell recruitment skews the results towards a more likely resolution of the infection by superimposing a fixed time for enabling T cell recruitment, as well as continuous unlimited availability of effector T cells, regardless of the level of infection in the lung. This highlights the use of tuneable resolution to identify a model flaw. Although the re-engineered *GRANSIM* (Figure 10c) gives more accurate predictions, computational efficiency is not affected (we are solving a single ODE that only occurs in one step of the model). In other work with a multi-organ model, however, tuneable resolution allowed a 17-fold increase in computational efficiency (49).

BOX:

Example Tuneable Resolution Algorithm. An overview of the algorithm used in simulations of the tuneable resolution multi-scale granuloma model with options for including TNF and NF- κ B submodels ($GRANSIM_{TNF}$ and $GRANSIM_{TNF-NFKB}$) (Examples 1 and 2). Rules and parameters for cell and bacteria processes (e.g. cell movement, cell recruitment, bacterial growth – Figure 6A) are the same between different resolutions of the model.



Discussion

Systems biologists are leveraging multi-scale modeling methods to study important biomedical problems in new ways. These models are exciting and we need new approaches to help with analyses, expand scientific and medical relevance, and promote sharing capabilities. We argue that developing and building models with tuneable resolution is a step in that direction. Tuneable resolution begins with a multi-scale model in place and strives to make model mechanisms more explanatory and thus more biomedically relevant, while simultaneously making them more useable and understandable. Our approach is applicable not only for systems that are multi-scale in space (including multi-organ) and time, but also for models that are multi-dimensional. In (97), for example, we develop an ABM of the LN that can be used in 2 or 3 dimensions.

Different features of the tuneable resolution approach that we describe here have been employed recently in other contexts. As examples, Gary An uses variable resolution components within a multi-scale model to explore and study the pathogenesis of multiple organ failure (100). An additional model use is enabling dynamic knowledge representation within the multi-scale model's modular architecture. Lam and Hunt (38) used sequential changes in micro-mechanism resolution to improve explanatory insight into the paradoxical roles of P-glycoprotein, Cyp3A4 enzymes, and sub-cellular microenvironments in determining temporal patterns of transport and metabolism of saquinavir (an antiretroviral drug) in Caco-2 cell cultures. Focusing on explanatory cell-level mechanisms of epithelial cell cystogenesis in cultures, Kim and Hunt (101) used resolution tuning to evolve fully rule-based cell agents into composite counterparts that achieved quantitative cross-model validation targets under normal and dysregulated conditions. Ruiz-Herrero et al. developed a coarse-grained model of receptor-ligand binding, allowing computationally efficient consideration of some spatial aspects of interactions (102). Tang et al. (14, 103, 104) altered the resolution of different multi-scale model components in order to enable dynamic simulation results to achieve quantitative validation targets drawn from a variety of different experimental conditions. It is useful to view all of these from within the framework of tuneable resolution provided here.

A current weakness of the tuneable resolution approach is that it is relatively new and in use in only a few laboratories. It is not yet clear how established good modeling and simulation practices will need to be expanded to cover the new methods. Figure 2 serves to highlight an issue for which additional best practice guidelines may be needed. During each tuning exercise, there are frequent opportunities to introduce bias, artefacts, and/or seed an inscription error (7, 105), (<http://furm.org/glossary.html>), which—if unnoticed—will jeopardize the scientific usefulness of subsequent model refinements. The risks are somewhat amplified because we are working in the green area of Figure 4, striving to move rightward. Consequently, the models are perpetual works in progress. The best mitigating

strategy is to reinforce adherence to good modeling and simulation practices, and that includes keeping records of tuning protocols, consequences, inferences, decisions, and evidence of feature falsification. The ideal course for model improvement (Figure 3) anticipates incremental tuning to expand both coarse- and fine-grain model overlap. However, tuning to improve overlap in one “direction” may come at the cost of reduced consistency in areas previously covered. A mitigating strategy is to expand the variety of qualitative (and, later, quantitative) validation targets and/or increase the variety of biomimetic constraints, and confirm through *in silico* experimentation that those targets are still achieved. Doing so, however, places an additional demand on modeler efforts. Because tuning is currently a hands-on activity, considerable time and effort may be required to successfully complete several tuning cycles, and that can be considered a shortcoming. A mitigating strategy is to increase modularity at both mechanism description and software levels so that refactoring decreases as explanatory power increases. The technical challenges faced when switching between coarse and fine grain components are common to all multi-scale modeling efforts and are well understood (7-9, 30-38, 59, 60). Consequently, efficient resolution tuning should be a priority requirement at the beginning of a project because it can influence selection of modeling methods.

We envision that the most efficient and productive path to more effective and eventually curative therapeutic intervention strategies for TB and other diseases will involve many cycles through the right side of Figure 1 coupled with the occasional but essential cycle through the left side. The approach can be extended to and beyond clinical trials. We anticipate new knowledge falsifying some model and/or assumption details, requiring feature revision and inclusion of new features. We do *not* anticipate those future virtual experiments, even those requiring virtual patients, to utilize a single, grand, unified multi-scale model, however. Because each virtual experiment will be motivated by a specific question or hypothesis, it will, like wet-lab counterparts, focus on just one (or at most a few) aspect of the disease and its context. As was the case for Examples 1-3, we expect the model used to be somewhat individualized (and somewhat optimized, from an execution perspective) for the particular virtual experiment and its uses: easily (ideally automatically) assembled from a family of exchangeable model components, each having achieved aspect-specific validation targets. Because TB phenomena are multi-scale within and across many aspects of the disease, we anticipate that many of those virtual experiments will require a resolution change one or more times during execution. Thus, we argue that having, expanding, and improving that capability is essential to achieving important public health outcomes from computational models.

A multi-scale model that has resolution-tuning capabilities and has earned a degree of credibility provides improved, plausible explanations of how events may coalesce into phenomena within and between biological scales. Such improved insight—improvement in the *theory* of TB, in our examples—is often infeasible to achieve

through wet-lab experimentation alone. The most frequently touted benefit of multi-scale modeling is improved predictions. We have demonstrated how improved scientific value can be derived from exploring and refining plausible, explanatory multi-scale mechanisms using a tuneable resolution approach.

Acknowledgements

This work was supported by NIH R01 HL106804 (DEK), R01 GM096040 (JJL), R01 EB012579 (DEK and JJL) and R01 HL 110811 (DEK and JJL).

Figures with captions

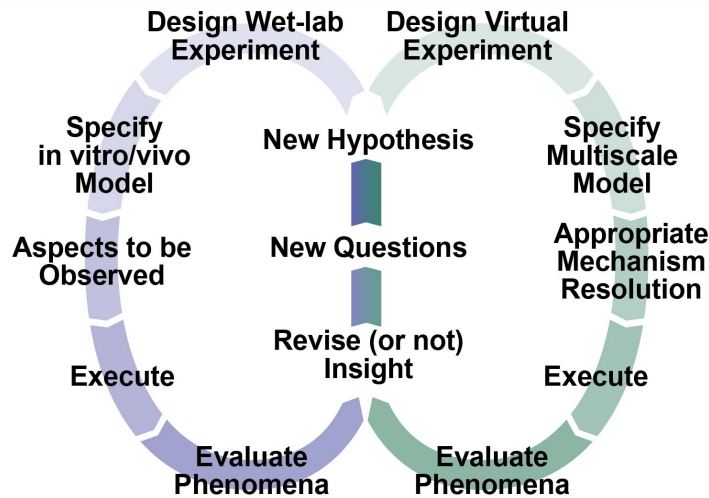


Figure 1. Coupled use of wet-lab and virtual experiments. Left side: scientific flow of wet-lab experiments from design through interpretation. Right side: Scientific flow of virtual experiments from design through interpretation. Two cycles intersect to generate hypotheses to pose and address new questions. Iteration is a key component of this process and involves multiple cycles on either or both sides.

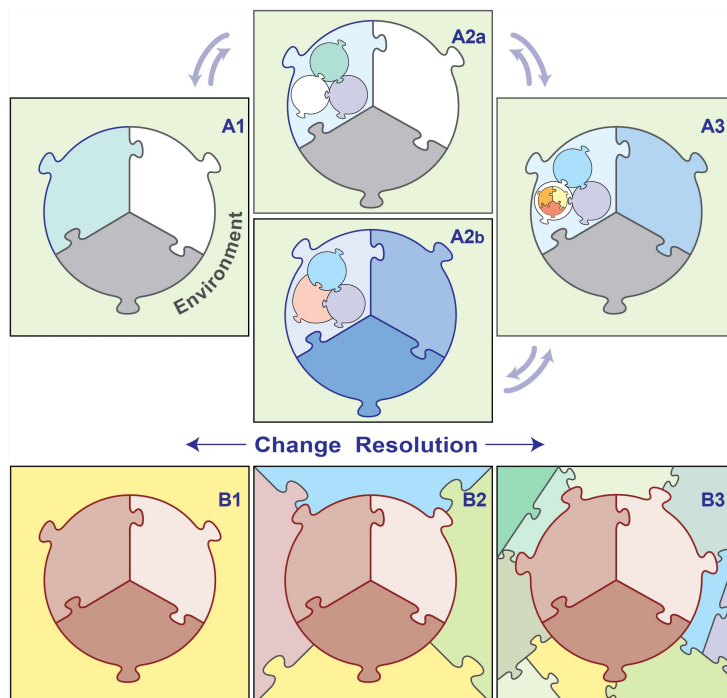


Figure 2. Tuneable resolution approach. (top) An initial model (shown as 3 puzzle pieces) functions within an environment (A1). Fine-graining a portion of the initial model to generate A2a, and subsequently a portion of that latter model to generate A3, adds additional scales of relevance. Progression from A3 to A2b demonstrates re-engineering of the previous scale model (A2a) to reflect knowledge gained at A3. (bottom) An initial model is refined to include additional scales of interest in the environment as model development progresses from B1 through B3. Depending on the question or aspect, the user chooses the appropriate level of resolution.

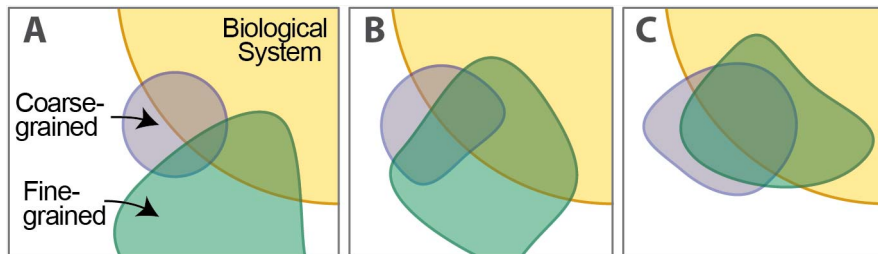


Figure 3. Comparing the behavior of multi-scale models (determined with virtual experiments) and the behavior of a biological system (determined with wet-lab experiments). The degree to which a model captures the biological system is represented by overlap between the model and biological system shapes (purple and yellow, or green and yellow). The degree to which the fine- and coarse-grained models predict the same behavior is represented by overlap between the purple and green shapes. In order to toggle between the two models to simulate resolution tuning, acceptable similarities (sufficient congruency) for the same set of phenomena must be observed. After initial sensitivity and uncertainty analyses, phenomena overlap between the sibling models is typically inadequate, indicating that further refinements are needed, possibly in both models, providing a degree of cross-model validation (Panels A to C). Because the two model versions are not the same, we should not expect complete overlap across their full range of realizations. Hayenga et al. (106) provide an instructive demonstration of achieving congruency between an agent-based and a continuum-based biomechanical model.

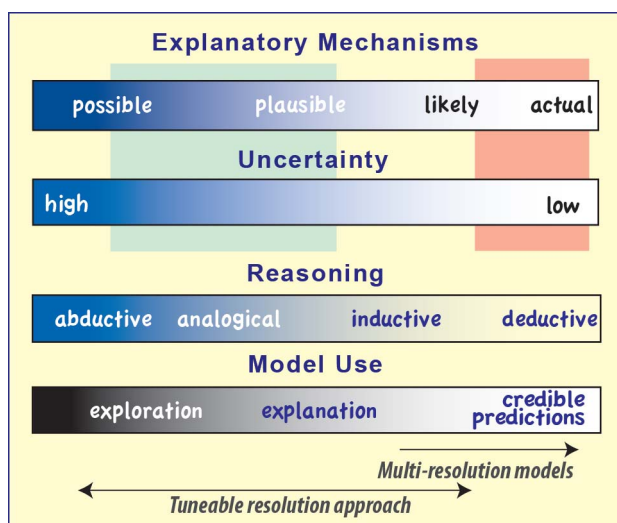


Figure 4. These four spectra inform modeling approaches, help characterize how multi-scale models can and should be used within the larger biomedical context, and

help distinguish our tuneable resolution approach from multi-resolution modeling. Locations on the top two spectra characterize the current state of knowledge about biological systems and phenomena of interest. For immune responses to TB and other diseases, the locations selected typically fall within the green box (top left). The pink area characterizes systems for which trusted, fine-grained explanatory mechanisms are available at the highest level of resolution needed for envisioning multi-scale model uses.

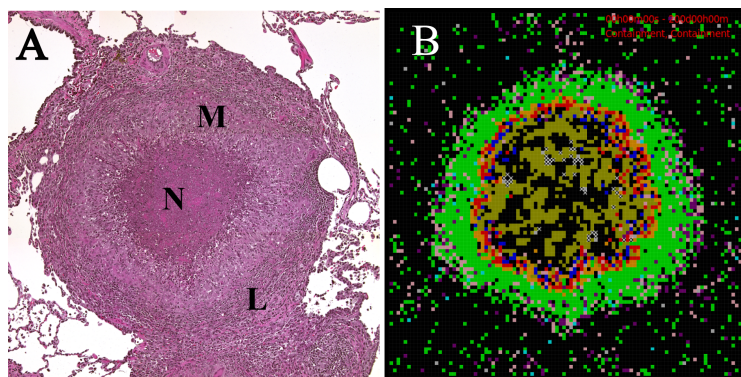


Figure 5: Non-human primate and simulated granulomas. (A) Histopathology of a granuloma in a primate infected with *M. tuberculosis* at ~30 weeks post infection (courtesy of JoAnne Flynn, University of Pittsburgh). This typical caseous granuloma shows central necrosis (N) surrounded by macrophages (M) and an outer cuff of lymphocytes (T cells) (L). (B) Snapshot of a simulated TB granuloma at 200 days post infection. Cell types: macrophages (resting-green, activated-blue, infected-orange, chronically infected-red), effector lymphocytes (pro-inflammatory IFN- γ producing T cells-T $_{\gamma}$ in pink, cytotoxic T cell-T $_c$ in purple, regulatory T cell-T $_{reg}$ in light blue), extracellular bacteria (olive green), vascular sources-grey, necrotic spots (x). The granuloma shown in Panel B has a total bacterial load of $\sim 2 \times 10^5$ *M. tuberculosis*, mostly extracellular, proliferating and located in the necrotic core.

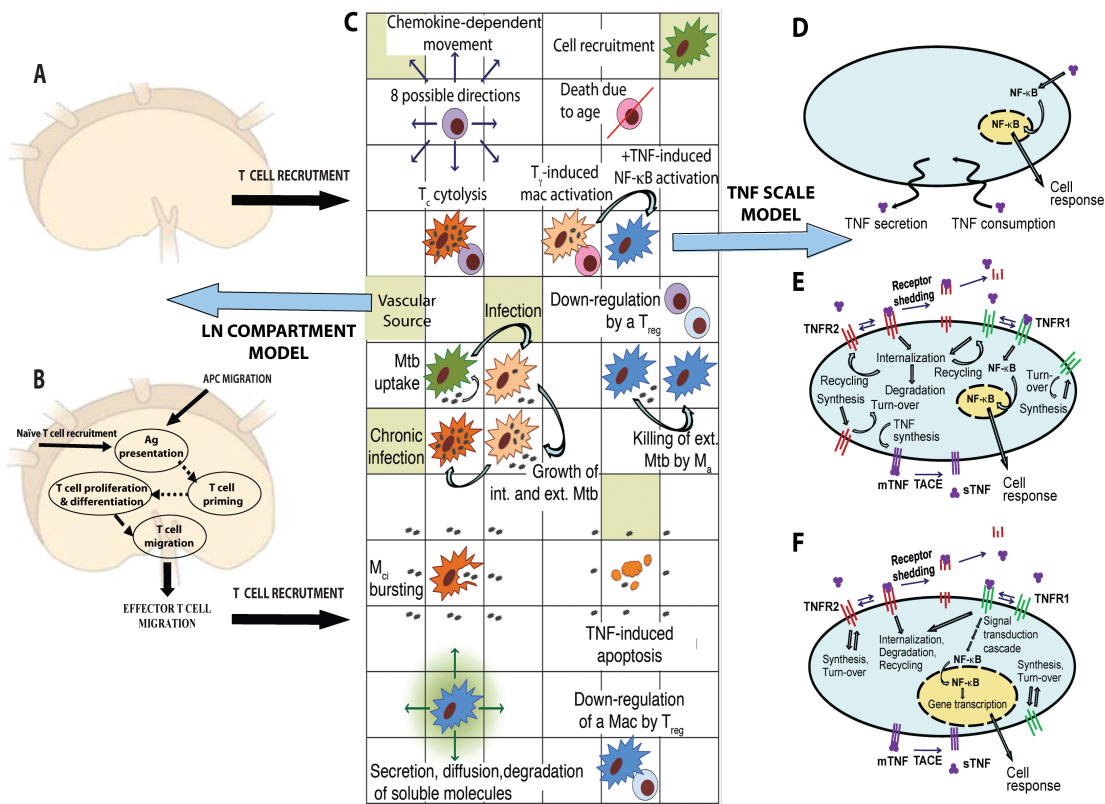


Figure 6: Schematic representation of the multi-scale multi-compartment model of the immune response to *M. tuberculosis* infection. Panel A shows an overview of selected ABM rules of interaction between host cells, bacteria and lung environment as implemented in GRANSIM (69, 70), which focuses on cellular and tissue scale dynamics. Panels B-D illustrate a molecular scale TNF sub-model that can be embedded at three levels of resolution (coarse (B), intermediate (C), fine (D)) in GRANSIM. The molecular scale model for TNF (Panel C) is described in (11) and when implemented in the granuloma model is termed GRANSIM_{TNF} (Example 1). The molecular scale model for NF-κB (Panel D) is described in (82) and when implemented in the granuloma model is termed GRANSIM_{TNF-NFKB} (Example 2). In Panels E-F the lymph node (LN) dynamics are described as in (94) at two levels of resolution (coarse (E), fine (F)) (Example 3). Abbreviations: *M. tuberculosis* (M_{tbc}), macrophage (mac), antigen (Ag), chronically infected macrophage (M_{ci}), activated macrophage (M_a), pro-inflammatory IFN-γ producing T cell (T_y) cytotoxic T cell (T_c), regulatory T cell (T_{reg}), TNF-a converting enzyme (TACE), TNF receptor types 1 and 2 (TNFR1, TNFR2), membrane and soluble forms of TNF (mTNF, sTNF).

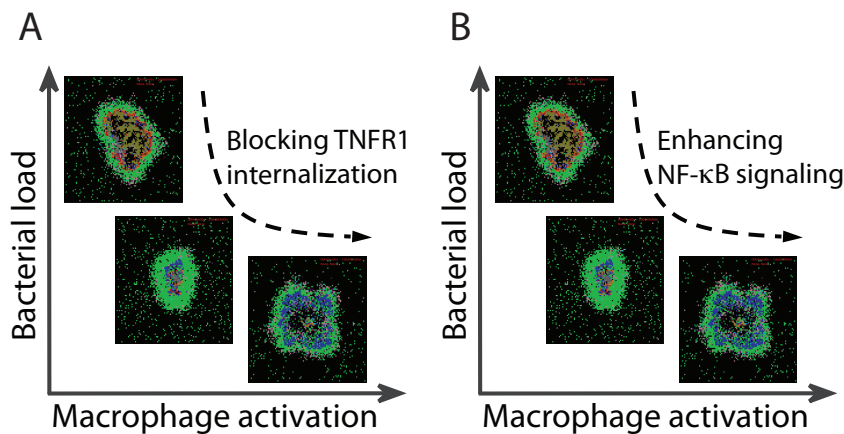


Figure 7. Congruent behaviors achieved from two model resolutions. The predicted roles of TNF internalization and NF- κ B signaling in determining granuloma outcomes are shown. Simulations with $GRANSIM_{TNF}$ (Example 1) show that reducing TNFR1 internalization enhances bacterial killing and increases the probability of bacterial clearance. However, the increased TNF concentrations that result give rise to excessive macrophage activation and increased tissue inflammation. Simulations with $GRANSIM_{TNF-NFKB}$ (Example 2) show that containment of bacteria is achieved when a balance exists between the NF- κ B-mediated bacterial killing activities and the NF- κ B-mediated inflammation. These levels of model resolution are well-suited to exploring potential pharmacological interventions of the signaling pathway. Snapshots of granulomas follow the same color mapping for cells as in Figure 5. The range of behaviors simulated with the two resolutions shows model congruency (see Figure 3).

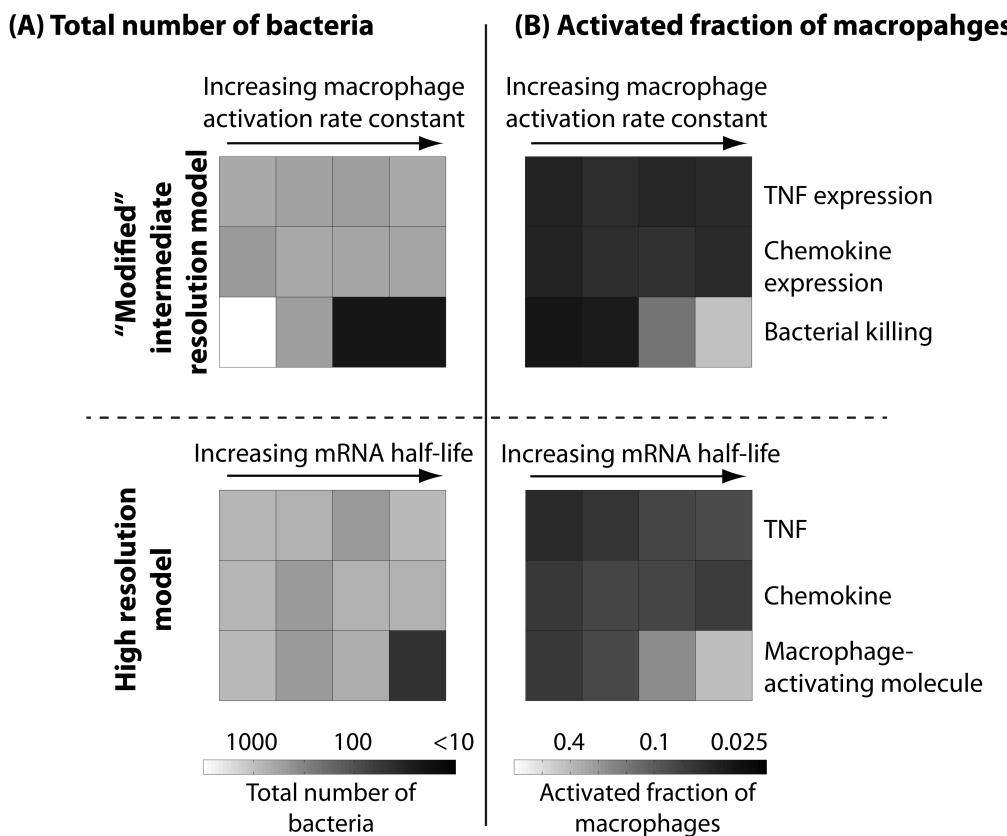


Figure 8. Refinement of $GRANSIM_{TNF}$. Using uncertainty and sensitivity analyses and knowledge gained from $GRANSIM_{TNF-NFKB}$, the intermediate resolution model $GRANSIM_{TNF}$ was improved to capture the effects of timing of different NF- κ B mediated responses on granuloma formation. Simulation results are shown for the effect of the timing of NF- κ B-mediated responses, including macrophage activation to efficiently kill bacteria, TNF expression, and chemokine expression on (A) bacteria numbers 200 days post-infection and (B) activated fraction of macrophages 50 days post-infection. Bottom panels show results from $GRANSIM_{TNF-NFKB}$ in which the timing of NF- κ B-mediated responses is regulated by their corresponding RNA stabilities (half-lives). Simulations are run varying the stability of mRNA transcripts corresponding to macrophage-activating molecules, chemokines and TNF while maintaining the average extent of the responses at their containment baseline levels (82). To maintain the average extent of each response as its corresponding mRNA stability is varied, we simultaneously vary another parameter associated with a process downstream of mRNA translation. Parameters varied to adjust the extent of the three NF- κ B mediated responses are: TNF secretion rate, chemokine secretion rate, ACT concentration threshold for macrophage activation, and macrophage activation rate constant. Four values of mRNA half-life were tested in fine-grain simulations: 12 min, 30 min, 1 hr and 3hr. Top panels show results from the modified $GRANSIM_{TNF}$ in which the timing of NF- κ B-mediated responses is regulated by new parameters $k_{activation}$, $k_{chemokine}$, and k_{TNF} . Four values tested for each of these three parameters in intermediate resolution simulations are: 1.26×10^{-8} , 3.97×10^{-8} , and 1.26×10^{-7} and 3.97×10^{-7} ($\#/cell$) $^{-1}s^{-1}$. All other parameters are kept at their containment (baseline) levels. Simulation results are averaged over 10 repetitions.

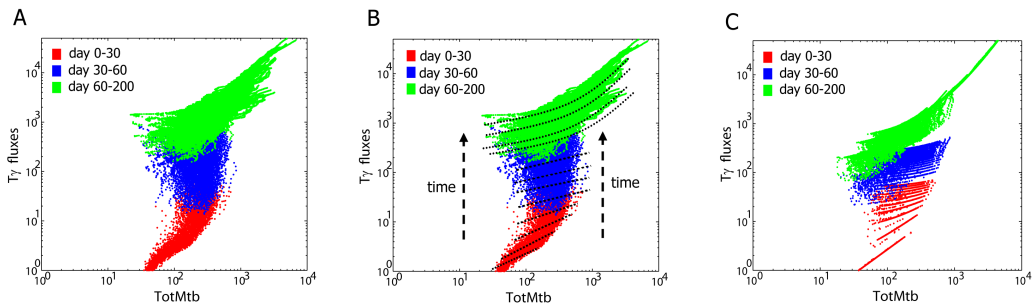


Figure 9. Comparisons of $T\gamma$ cell fluxes (y-axis) across different resolutions. T cells that make the cytokine IFN- γ ($T\gamma$) are shown on the y-axis. The x-axis represents total bacteria count (TotMtb). Each plot displays a total of 900x200 points. Each point is the combination of total bacteria count and $T\gamma$ cell fluxes at a certain day during a simulated 200-day infection. Different colors correspond to different time intervals. **A:** results using the fine-grained version of T cell recruitment ($GRANSIM-LN$). **B:** the data from **A** with examples of linear and quadratic functions superimposed to fit the data. **C:** results using the improved coarse-grained model in which the fine-grained fluxes in **A** are approximated using the linear and quadratic functions illustrated in **B**. For days 0-60, we use linear approximations. For days 60-200 we use quadratic functions. We fit simulated $T\gamma$ and T_C fluxes separately. In order to cross-validate with fine-grained LN outcome distributions, we truncated the approximations at a certain level of total bacteria, below which the flux becomes 0. For example after day 30, if bacteria < 35, fluxes are set to 0.

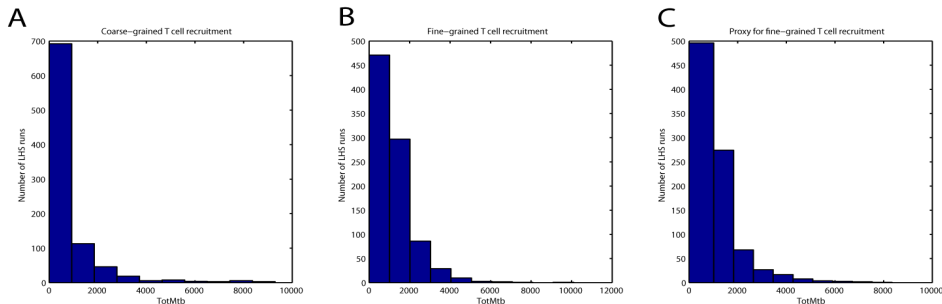


Figure 10. Histograms illustrating outcome distributions across different model resolutions. Total bacteria count at day 200 is used as proxy for TB outcome (x-axis). Each plot displays a total of 900 outcomes (i.e., 900 different parameter combinations) resulting from the VEs described in the text. Each point is the combination of total bacterial count and $T\gamma$ cell fluxes at a certain day during simulated infection. (A): T cell recruitment using GRANSIM. (B): T cell recruitment using GRANSIM-LN. (C): T cell recruitment using re-engineered GRANSIM.

Related Articles

Article ID [or Subtopic]	Article title
WSBM.in press	Chylek, L. et al. 2013. Rule-based modeling: a computational approach for studying biomolecular site dynamics in cell signaling systems. <i>WIREs System Biology and Medicine</i>
WSBM.1222	Hunt et al. 2013. Agent-based modelling: a systematic assessment of use cases and requirements for enhancing pharmaceutical research and development productivity June 1, 2013
WSBM.45	An et al. <u>Agent-based models in translational systems biology</u> 2009.

References

1. Bokulich, A. 2011. How scientific models can explain. *Synthese* 180:33-45
2. Darden, L. 2008. Thinking Again about Biological Mechanisms. *Philos Sci* 75:958-969
3. Weiskopf, D. A. 2011. Models and mechanisms in psychological explanation. *Synthese* 183:313-338
4. Craver, C. F. 2006. When mechanistic models explain. *Synthese* 153:355-376
5. Winther, R. G. 2012. Interweaving categories: Styles, paradigms, and models. *Studies in History and Philosophy of Science Part A* 43:628-639
6. Weisberg, M. 2013. *Simulation and Similarity: Using Models to Understand the World (Oxford Studies in Philosophy of Science)*. Oxford University Press, New York.
7. Hunt, C. A., G. P. Ropella, T. Lam, J. Tang, S. J. Kim, J. Engelberg, and S. Sheikh-Bahaei. 2009. At the Biological Modeling and Simulation Frontier. *Pharm Res* 26:2369-2400
8. Hunt, C. A., and G. E. P. Ropella. 2011. Moving beyond in silico tools to in silico science in support of drug development research. *Drug Development Research* 72:153-161
9. Hunt, C. A., R. C. Kennedy, S. H. J. Kim, and G. E. P. Ropella. 2013. Agent-based modeling: a systematic assessment of use cases and requirements for enhancing pharmaceutical

- research and development productivity. *Wiley Interdisciplinary Reviews: Systems Biology and Medicine* 5:461-480
- 10. de Lara, J., and H. Vangheluwe. 2002. AToM(3): A tool for multi-formalism and meta-modelling. *Lect Notes Comput Sc* 2306:174-188
 - 11. Fallahi-Sichani, M., M. El-Kebir, S. Marino, D. E. Kirschner, and J. J. Linderman. 2011. Multiscale computational modeling reveals a critical role for TNF-alpha receptor 1 dynamics in tuberculosis granuloma formation. *J Immunol* 186:3472-3483
 - 12. Han, L. Q., J. Hanan, and P. M. Gresshoff. 2010. Computational Complementation: A Modelling Approach to Study Signalling Mechanisms during Legume Autoregulation of Nodulation. *Plos Comput Biol* 6
 - 13. Karalis, V., A. Dokoumetzidis, and P. Macheras. 2004. A physiologically based approach for the estimation of recirculatory parameters. *J Pharmacol Exp Ther* 308:198-205
 - 14. Tang, J., and C. A. Hunt. 2010. Identifying the rules of engagement enabling leukocyte rolling, activation, and adhesion. *Plos Comput Biol* 6:e1000681
 - 15. Park, S., G. E. Ropella, S. H. Kim, M. S. Roberts, and C. A. Hunt. 2009. Computational strategies unravel and trace how liver disease changes hepatic drug disposition. *The Journal of pharmacology and experimental therapeutics* 328:294-305
 - 16. Fallahi-Sichani, M., S. Marino, J. L. Flynn, J. J. Linderman, and D. E. Kirschner. 2012. A systems biology approach for understanding granuloma formation and function in tuberculosis. In *Systems biology of tuberculosis*. D. B. a. A. K. J. McFadden, ed. Springer.
 - 17. Bassingthwaigte, J. B., D. A. Beard, B. E. Carlson, R. K. Dash, and K. Vinnakota. 2012. Modeling to link regional myocardial work, metabolism and blood flows. *Ann Biomed Eng* 40:2379-2398
 - 18. Beard, D. A., M. L. Neal, N. Tabesh-Saleki, C. T. Thompson, J. B. Bassingthwaigte, M. Shimoyama, and B. E. Carlson. 2012. Multiscale modeling and data integration in the virtual physiological rat project. *Ann Biomed Eng* 40:2365-2378
 - 19. Bolser, D. C., T. E. Pitts, and K. F. Morris. 2011. The use of multiscale systems biology approaches to facilitate understanding of complex control systems for airway protection. *Curr Opin Pharmacol* 11:272-277
 - 20. Campbell, S. G., and A. D. McCulloch. 2011. Multi-scale computational models of familial hypertrophic cardiomyopathy: genotype to phenotype. *J R Soc Interface* 8:1550-1561
 - 21. Flamm, M. H., and S. L. Diamond. 2012. Multiscale systems biology and physics of thrombosis under flow. *Ann Biomed Eng* 40:2355-2364
 - 22. Kim, E., S. Stamatelos, J. Cebulla, Z. M. Bhujwalla, A. S. Popel, and A. P. Pathak. 2012. Multiscale imaging and computational modeling of blood flow in the tumor vasculature. *Ann Biomed Eng* 40:2425-2441
 - 23. Politi, A. Z., G. M. Donovan, M. H. Tawhai, M. J. Sanderson, A. M. Lauzon, J. H. Bates, and J. Sneyd. 2010. A multiscale, spatially distributed model of asthmatic airway hyper-responsiveness. *J Theor Biol* 266:614-624
 - 24. Vodovotz, Y., M. Csete, J. Bartels, S. Chang, and G. An. 2008. Translational systems biology of inflammation. *Plos Comput Biol* 4:e1000014
 - 25. Walpole, J., J. A. Papin, and S. M. Peirce. 2013. Multiscale computational models of complex biological systems. *Annu Rev Biomed Eng* 15:137-154
 - 26. Wang, W., and M. R. King. 2012. Multiscale modeling of platelet adhesion and thrombus growth. *Ann Biomed Eng* 40:2345-2354
 - 27. Coveney, P. V., and P. W. Fowler. 2005. Modelling biological complexity: a physical scientist's perspective. *J R Soc Interface* 2:267-280
 - 28. Kirschner, D. 2007. The multi-scale immune response to pathogens: M. tuberculosis as an example. In *In silico Immunology*. D. Flower, and J. Timmis, eds. Springer, New York. 289-311.
 - 29. Vlachos, D. G. 2005. A review of multiscale analysis: Examples from systems biology, materials engineering, and other fluid-surface interacting systems. *Adv. Chem. Eng.*:30-31

30. Alden, K., M. Read, J. Timmis, P. S. Andrews, H. Veiga-Fernandes, and M. Coles. 2013. Spartan: A Comprehensive Tool for Understanding Uncertainty in Simulations of Biological Systems. *Plos Comput Biol* 9
31. Bhalla, U. S., and R. Iyengar. 1999. Emergent properties of networks of biological signaling pathways. *Science* 283:381-387
32. Chylek, L. A., L. A. Harris, C. S. Tung, J. R. Faeder, C. F. Lopez, and W. S. Hlavacek. 2013. Rule-based modeling: a computational approach for studying biomolecular site dynamics in cell signaling systems. *Wiley Interdiscip Rev Syst Biol Med*
33. Hlavacek, W. S., J. R. Faeder, M. L. Blinov, A. S. Perelson, and B. Goldstein. 2003. The complexity of complexes in signal transduction. *Biotechnol Bioeng* 84:783-794
34. Hlavacek, W. S., J. R. Faeder, M. L. Blinov, R. G. Posner, M. Hucka, and W. Fontana. 2006. Rules for modeling signal-transduction systems. *Sci STKE* 2006:re6
35. Kholodenko, B., M. B. Yaffe, and W. Kolch. 2012. Computational approaches for analyzing information flow in biological networks. *Sci Signal* 5:re1
36. Marchisio, M. A., M. Colaiacovo, E. Whitehead, and J. Stelling. 2013. Modular, rule-based modeling for the design of eukaryotic synthetic gene circuits. *BMC Syst Biol* 7:42
37. Vilar, J. M., and L. Saiz. 2013. Reliable Prediction of Complex Phenotypes from a Modular Design in Free Energy Space: An Extensive Exploration of the lac Operon. *ACS Synth Biol*
38. Lam, T. N., and C. A. Hunt. 2010. Mechanistic insight from in silico pharmacokinetic experiments: roles of P-glycoprotein, Cyp3A4 enzymes, and microenvironments. *J Pharmacol Exp Ther* 332:398-412
39. Angermann, B. R., F. Klauschen, A. D. Garcia, T. Prustel, F. Zhang, R. N. Germain, and M. Meier-Schellersheim. 2012. Computational modeling of cellular signaling processes embedded into dynamic spatial contexts. *Nat Methods* 9:283-289
40. Andasari, V., R. T. Roper, M. H. Swat, and M. A. Chaplain. 2012. Integrating intracellular dynamics using CompuCell3D and Bionetsolver: applications to multiscale modelling of cancer cell growth and invasion. *PLoS One* 7:e33726
41. Meier-Schellersheim, M., X. Xu, B. Angermann, E. J. Kunkel, T. Jin, and R. N. Germain. 2006. Key role of local regulation in chemosensing revealed by a new molecular interaction-based modeling method. *Plos Comput Biol* 2:e82
42. Donoho, D. L., A. Maleki, M. Shahram, I. U. Rahman, and V. Stodden. 2009. Reproducible Research in Computational Harmonic Analysis. *Comput Sci Eng* 11:8-18
43. Fomel, S., and G. Hennenfent. 2007. Reproducible computational experiments using SCons. *Int Conf Acoust Spee:1257-1260*
44. Mesirov, J. P. 2010. Accessible Reproducible Research. *Science* 327:415-416
45. Morin, A., J. Urban, P. D. Adams, I. Foster, A. Sali, D. Baker, and P. Sliz. 2012. Shining Light into Black Boxes. *Science* 336:159-160
46. Peng, R. D. 2009. Reproducible research and Biostatistics. *Biostatistics* 10:405-408
47. Stodden, V. 2010. The Scientific Method in Practice: Reproducibility in the Computational Sciences *MIT Sloan Research Paper* 4773:10
48. Marino, S., I. B. Hogue, C. J. Ray, and D. E. Kirschner. 2008. A methodology for performing global uncertainty and sensitivity analysis in systems biology. *J Theor Biol* 254:178-196
49. Gong, C., Linderman, JJ and Kirschner, DE. 2013. Harnessing the heterogeneity of T cell differentiation fate to fine-tune generation of effector and memory T cells. *Frontiers in Immunology* 5:57
50. Davis, P. K., and R. Hillestad. 1993. Families of Models That Cross Levels of Resolution - Issues for Design, Calibration and Management. *1993 Winter Simulation Conference Proceedings*:1003-1012
51. Natrajan, A., P. F. Reynolds, and S. Srinivasan. 1997. MRE: A flexible approach to multi-resolution modeling. *11th Workshop on Parallel and Distributed Simulation, Proceedings*:156-163

52. Bigelow, J. H., and P. K. Davis. 2002. Developing improved metamodels by combining phenomenological reasoning with statistical methods. *P Soc Photo-Opt Ins* 4716:167-180
53. Davis, P. K. 2000. Exploratory analysis enabled by multiresolution, multiperspective modeling. *Proceedings of the 2000 Winter Simulation Conference, Vols 1 and 2*:293-302
54. Kasputis, S., and H. C. Ng. 2000. Composable simulations. *Proceedings of the 2000 Winter Simulation Conference, Vols 1 and 2*:1577-1584
55. Aumann, C. A. 2007. A methodology for developing simulation models of complex systems. *Ecol Model* 202:385-396
56. Kimmins, J. P., J. A. Blanco, B. Seely, C. Welham, and K. Scoullar. 2008. Complexity in modelling forest ecosystems: How much is enough? *Forest Ecol Manag* 256:1646-1658
57. Ratze, C., F. Gillet, J. P. Muller, and K. Stoffel. 2007. Simulation modelling of ecological hierarchies in constructive dynamical systems. *Ecol Complex* 4:13-25
58. Wu, J. G., and J. L. David. 2002. A spatially explicit hierarchical approach to modeling complex ecological systems: theory and applications. *Ecol Model* 153:7-26
59. Bassingthwaite, J. B., H. J. Chizeck, and L. E. Atlas. 2006. Strategies and Tactics in Multiscale Modeling of Cell-to-Organ Systems. *Proceedings of the IEEE* 94:819-831
60. Hernandez, A. I., V. Le Rolle, A. Defontaine, and G. Carrault. 2009. A multiformalism and multiresolution modelling environment: application to the cardiovascular system and its regulation. *Philos T R Soc A* 367:4923-4940
61. Brenner, S., Noble, Denis, Sejnowski, Terrence J., et al. 2001. Understanding complex systems: top-down, bottom-up or middleout? In *Novartis Foundation Symposium: Complexity in Biological Information Processing*. G. G. Bock, J., ed. Wiley. 150-159.
62. Bokulich, A. 2013. Explanatory Models Versus Predictive Models: Reduced Complexity Modeling in Geomorphology. In *EPSA11 Perspectives and Foundational Problems in Philosophy of Science*. D. D. Vassilios Karakostos, ed. Springer International Publishing. 115-128.
63. Viceconti, M. 2011. A tentative taxonomy for predictive models in relation to their falsifiability. *Philos Trans A Math Phys Eng Sci* 369:4149-4161
64. Hunt, C. A., G. E. Ropella, T. Lam, and A. D. Gewitz. 2011. Relational grounding facilitates development of scientifically useful multiscale models. *Theor Biol Med Model* 8:35
65. Bartha, P. 2013. Analogy and Analogical Reasoning. In *The Stanford Encyclopedia of Philosophy (Fall Edition)*. E. N. Zalta, ed. The Metaphysics Research Lab, Center for the Study of Language and Information, Standford. <http://plato.stanford.edu/archives/fall2013/entries/reasoning-analogy/>.
66. Conzelmann, H., J. Saez-Rodriguez, T. Sauter, E. Bullinger, F. Allgower, and E. D. Gilles. 2004. Reduction of mathematical models of signal transduction networks: simulation-based approach applied to EGF receptor signalling. *Syst Biol (Stevenage)* 1:159-169
67. Maurya, M. R., S. J. Bornheimer, V. Venkatasubramanian, and S. Subramaniam. 2005. Reduced-order modelling of biochemical networks: application to the GTPase-cycle signalling module. *Syst Biol (Stevenage)* 152:229-242
68. Maurya, M. R., S. Katare, P. R. Patkar, A. E. Rundell, and V. Venkatasubramanian. 2006. A systematic framework for the design of reduced-order models for signal transduction pathways from a control theoretic perspective. *Computers & Chemical Engineering* 30:437-452
69. Segovia-Juarez, J. L., S. Ganguli, and D. Kirschner. 2004. Identifying control mechanisms of granuloma formation during *M. tuberculosis* infection using an agent-based model. *J Theor Biol* 231:357-376
70. Ray, J. C., J. L. Flynn, and D. E. Kirschner. 2009. Synergy between individual TNF-dependent functions determines granuloma performance for controlling *Mycobacterium tuberculosis* infection. *J Immunol* 182:3706-3717
71. Flynn, J. L., M. M. Goldstein, J. Chan, K. J. Triebold, K. Pfeffer, C. J. Lowenstein, R. Schreiber, T. W. Mak, and B. R. Bloom. 1995. Tumor necrosis factor-alpha is required in the protective immune response against *Mycobacterium tuberculosis* in mice. *Immunity* 2:561-572

72. Saunders, B. M., H. Briscoe, and W. J. Britton. 2004. T cell-derived tumour necrosis factor is essential, but not sufficient, for protection against *Mycobacterium tuberculosis* infection. *Clin Exp Immunol* 137:279-287
73. Algood, H. M., P. L. Lin, D. Yankura, A. Jones, J. Chan, and J. L. Flynn. 2004. TNF influences chemokine expression of macrophages in vitro and that of CD11b+ cells in vivo during *Mycobacterium tuberculosis* infection. *J Immunol* 172:6846-6857
74. Keane, J., M. K. Balcewicz-Sablinska, H. G. Remold, G. L. Chupp, B. B. Meek, M. J. Fenton, and H. Kornfeld. 1997. Infection by *Mycobacterium tuberculosis* promotes human alveolar macrophage apoptosis. *Infect Immun* 65:298-304
75. Harris, J., J. C. Hope, and J. Keane. 2008. Tumor Necrosis Factor Blockers Influence Macrophage Responses to *Mycobacterium tuberculosis*. *J Infect Dis* 198:1842-1850
76. Lin, P. L., A. Myers, L. Smith, C. Bigbee, M. Bigbee, C. Fuhrman, H. Grieser, I. Chiosea, N. N. Voitenek, S. V. Capuano, E. Klein, and J. L. Flynn. 2010. Tumor necrosis factor neutralization results in disseminated disease in acute and latent *Mycobacterium tuberculosis* infection with normal granuloma structure in a cynomolgus macaque model. *Arthritis Rheum* 62:340-350
77. Wallis, R. S. 2009. Infectious complications of tumor necrosis factor blockade. *Curr Opin Infect Dis* 22:403-409
78. Wallis, R. S., M. S. Broder, J. Y. Wong, M. E. Hanson, and D. O. Beenhouwer. 2004. Granulomatous infectious diseases associated with tumor necrosis factor antagonists. *Clin Infect Dis* 38:1261-1265
79. Tubach, F., D. Salmon, P. Ravaud, Y. Allanore, P. Goupille, M. Breban, B. Pallot-Prades, S. Pouplin, A. Sacchi, R. M. Chichemanian, S. Bretagne, D. Emilie, M. Lemann, O. Lortholary, and X. Mariette. 2009. Risk of tuberculosis is higher with anti-tumor necrosis factor monoclonal antibody therapy than with soluble tumor necrosis factor receptor therapy: The three-year prospective French Research Axed on Tolerance of Biotherapies registry. *Arthritis Rheum* 60:1884-1894
80. Lin, P. L., H. L. Plessner, N. N. Voitenok, and J. L. Flynn. 2007. Tumor necrosis factor and tuberculosis. *J Investig Dermatol Symp Proc* 12:22-25
81. Fallahi-Sichani, M., M. A. Schaller, D. E. Kirschner, S. L. Kunkel, and J. J. Linderman. 2010. Identification of key processes that control tumor necrosis factor availability in a tuberculosis granuloma. *Plos Comput Biol* 6:e1000778
82. Fallahi-Sichani, M., J. L. Flynn, J. J. Linderman, and D. E. Kirschner. 2012. Differential risk of tuberculosis reactivation among anti-TNF therapies is due to drug binding kinetics and permeability. *J Immunol* 188:3169-3178
83. Cilfone, N. A., C. R. Perry, D. E. Kirschner, and J. J. Linderman. 2013. Multi-Scale Modeling Predicts a Balance of Tumor Necrosis Factor-alpha and Interleukin-10 Controls the Granuloma Environment during *Mycobacterium tuberculosis* Infection. *PLoS One* 8:e68680
84. Gutierrez, M. G., B. B. Mishra, L. Jordao, E. Elliott, E. Anes, and G. Griffiths. 2008. NF-kappa B activation controls phagolysosome fusion-mediated killing of mycobacteria by macrophages. *Journal of immunology* 181:2651-2663
85. Mosser, D. M., and J. P. Edwards. 2008. Exploring the full spectrum of macrophage activation. *Nat Rev Immunol* 8:958-969
86. Beg, A. A., and D. Baltimore. 1996. An essential role for NF-kappaB in preventing TNF-alpha-induced cell death. *Science* 274:782-784
87. Van Antwerp, D. J., S. J. Martin, T. Kafri, D. R. Green, and I. M. Verma. 1996. Suppression of TNF-alpha-induced apoptosis by NF-kappaB. *Science* 274:787-789
88. Tay, S., J. J. Hughey, T. K. Lee, T. Lipniacki, S. R. Quake, and M. W. Covert. 2010. Single-cell NF-kappaB dynamics reveal digital activation and analogue information processing. *Nature* 466:267-271
89. Karin, M., and A. Lin. 2002. NF-kappaB at the crossroads of life and death. *Nat Immunol* 3:221-227

90. Chackerian, A. A., J. M. Alt, T. V. Perera, C. C. Dascher, and S. M. Behar. 2002. Dissemination of *Mycobacterium tuberculosis* is influenced by host factors and precedes the initiation of T-cell immunity. *Infect Immun* 70:4501-4509
91. Chang, S. T., J. J. Linderman, and D. E. Kirschner. 2005. Multiple mechanisms allow *Mycobacterium tuberculosis* to continuously inhibit MHC class II-mediated antigen presentation by macrophages. *Proc Natl Acad Sci U S A* 102:4530-4535
92. Giacomini, E., E. Iona, L. Ferroni, M. Miettinen, L. Fattorini, G. Orefici, I. Julkunen, and E. M. Coccia. 2001. Infection of human macrophages and dendritic cells with *Mycobacterium tuberculosis* induces a differential cytokine gene expression that modulates T cell response. *J Immunol* 166:7033-7041
93. Hickman, S. P., J. Chan, and P. Salgame. 2002. *Mycobacterium tuberculosis* induces differential cytokine production from dendritic cells and macrophages with divergent effects on naive T cell polarization. *J Immunol* 168:4636-4642
94. Marino, S., M. El-Kebir, and D. Kirschner. 2011. A hybrid multi-compartment model of granuloma formation and T cell priming in Tuberculosis. *J Theor Biol* 280:50-62
95. Marino, S., A. Myers, J. L. Flynn, and D. E. Kirschner. 2010. TNF and IL-10 are major factors in modulation of the phagocytic cell environment in lung and lymph node in tuberculosis: a next-generation two-compartmental model. *J Theor Biol* 265:586-598
96. Garcia-Ramallo, E., T. Marques, N. Prats, J. Beleta, S. L. Kunkel, and N. Godessart. 2002. Resident cell chemokine expression serves as the major mechanism for leukocyte recruitment during local inflammation. *J Immunol* 169:6467-6473
97. Gong, C., J. T. Mattila, M. Miller, J. L. Flynn, J. J. Linderman, and D. Kirschner. 2013. Predicting lymph node output efficiency using systems biology. *J Theor Biol* 335C:169-184
98. Linderman, J. J., T. Riggs, M. Pande, M. Miller, S. Marino, and D. E. Kirschner. 2010. Characterizing the dynamics of CD4+ T cell priming within a lymph node. *J Immunol* 184:2873-2885
99. Riggs, T., A. Walts, N. Perry, L. Bickle, J. N. Lynch, A. Myers, J. Flynn, J. J. Linderman, M. J. Miller, and D. E. Kirschner. 2008. A comparison of random vs. chemotaxis-driven contacts of T cells with dendritic cells during repertoire scanning. *J Theor Biol* 250:732-751
100. An, G. 2008. Introduction of an agent-based multi-scale modular architecture for dynamic knowledge representation of acute inflammation. *Theor Biol Med Model* 5:11
101. Kim, S. H., and C. A. Hunt. 2011. Composite cell agent model of epithelial culture in vitro. . In *Proceedings of the 2011 Workshop on Agent-Directed Simulation. Society for Computer Simulation International*:45-51
102. Ruiz-Herrero, T., J. Estrada, R. Guantes, and D. G. Miguez. 2013. A tunable coarse-grained model for ligand-receptor interaction. *Plos Comput Biol* 9:e1003274
103. Tang, J., K. F. Ley, and C. A. Hunt. 2007. Dynamics of in silico leukocyte rolling, activation, and adhesion. *BMC Syst Biol* 1:14
104. Tang, J., I. Fernandez-Garcia, S. Vijayakumar, H. Martinez-Ruis, I. Illa-Bochaca, D. H. Nguyen, J. H. Mao, S. V. Costes, and M. H. Barcellos-Hoff. 2014. Irradiation of Juvenile, but not Adult, Mammary Gland Increases Stem Cell Self-Renewal and Estrogen Receptor Negative Tumors. *Stem Cells* 32:649-661
105. Smith, B. C. 1996. *On the Origin of Objects*. MIT Press, Cambridge.
106. Hayenga, H., B. Thorne, S. Peirce, and J. Humphrey. 2011. Ensuring Congruency in Multiscale Modeling: Towards Linking Agent Based and Continuum Biomechanical Models of Arterial Adaptation. *Ann Biomed Eng* 39:2669-2682